The Effect of using Gamma Titanium RF Electrodes on the Ablation Volume during the Radiofrequency Ablation Process

Mohammed S. Ahmed [1], Mohamed Tarek El-Wakad [2], Mohammed A. Hassan[3],
Mohammed.Sherif@h-eng.helwan.edu.eg mohamed.elwakad@fue.edu.eg mohammed.ali@h-eng.helwan.edu.eg
Department of Biomedical Engineering-Faculty of Engineering, Helwan University, Cairo, Egypt[1]
Department of Biomedical Engineering-Faculty of Engineering & Technology, Future University in Egypt, Cairo, Egypt[2]
Department of Biomedical Engineering-Faculty of Engineering, Helwan University, Cairo, Egypt[3]

Abstract
Radiofrequency ablation (RFA) is an alternative treatment for liver cancer to the surgical intervention preferred by surgeons. However, the main challenge remains the use of RF for the ablation of large tumours (i.e., tumours with a diameter of >3 cm). For large tumours, RFA takes a large duration in the ablation process compared with surgery, which increases patient pain. Therefore, RFA for large tumours is not preferred by surgeons. The currently materials used in RF electrodes, such as the nickel-titanium alloy (nitinol), are characterized by low thermal and electrical conductivities. On the other hand, the use of materials that have high thermal and electrical conductivities, such as titanium aluminide alloy (gamma titanium), produces more thermal energy for tumours. In this paper, we developed a cool-tip RF electrode model that uses nickel-titanium alloy and replaced it with titanium aluminide alloy by using the finite element model (FEM). The aim of this paper is to study the effect of the thermal and electrical conductivities of gamma titanium on the ablation volume. Results showed that the proposed design of the electrode increased the ablation rate by 1 cm^3 /minute and 6.3 cm^3/10 minutes, with a decrease in the required time ablation. Finally, the proposed model reduces the ablation time and damages healthy tissue while increasing the ablation volume from 22.5% cm^3 to 62.5% cm^3 in ten minutes compared to recent studies.

Keywords:
Radiofrequency ablation (RFA), Finite element model (FEM), COMSOL, Cool-tip RF

1. Introduction

Liver cancer is one of the leading causes of death in both developed and developing countries. It is ranked as the fifth in terms of the most common prevalence and as the third in terms of causes of cancer-related death [1]. It is treated by surgical resection and (RFA) [2]. However, for large tumors, it is not preferred but surgical resection is the preferred method [3]. Surgical resection isn't suitable for all patients due to multifocal disease, tumor size, and location of the tumor in relation to key vessels [4]. But on the other hand, for small tumors (i.e.,<3 cm in diameter), it is common to use RFA and other ablation methods such as microwave [5]. The RFA technique is the application of radiofrequency (RF) electrical signals to soft tissue [6]. RF electrodes are injected into the organ to generate enough RF joule heating to raise the temperature above 50° [7]. Tissues exposed to those temperatures for 1 minute or higher are destroyed by the heat [8]. This technique utilizes RF current (450-500 kHz) to generate a thermal field required to remove a liver tumor [9]. This current passes through the organ from the active electrode to the passive electrode [10]. There are two different types of RFA techniques depending on the placement of the passive electrode: bipolar or monopolar [11].

In the bipolar technique, electrical current passes between the two electrodes applied to the target tissue [12]. Bipolar applications are efficacious treatments for dermal defects, obesity, and sagging skin [13]. In the monopolar technique, the electrical current is connected to the organ through a small active electrode inserted into the tumor and a large electrode already present on the back of the patient [14, 15]. An RF voltage is generated by an RF generator between a reference electrode and the active electrode. The electric field oscillates the alternating radio current, causing oscillatory motion of ions in the tissue commensurate with the field intensity [16, 17]. Heating of tissue happens as a result of ionic excitation associated with the passage of RF current through the tissue [18]. The heat generation of tissue leads to cell dying by thermal coagulative necrosis. Therefore, RF volume thermal ablation is subject to the distribution of temperature in the tissue [19, 20]. For large tumors in general, the bipolar technique is used to achieve a larger ablation volume [21]. As a result, we chose the bipolar technique because our paper focuses on large tumors. Currently, most of the commonly used RF electrodes are made of nickel-titanium alloy [22]. Nickel-titanium alloy is a very good material for medical devices because it is biocompatible with the human body [23]. However, the main limitation with nickel-titanium alloy is its low thermal and electrical conductivities

Manuscript received February 5, 2023
Manuscript revised February 20, 2023
https://doi.org/10.22937/IJCSNS.2023.23.2.20

[24]. Electrodes made of materials with high thermal and electrical conductivity such as gamma titanium can contribute to increased ablation volume and reduced ablation time [25].

RFA can be used for a greater number of patients and it has a greater potential for repeated treatment of tumors compared to traditional surgical resection [26, 27]. The finite element model (FEM) is a numerical method used to approximate the solution of boundary and initial value problems characterized by partial differential equations [28]. Lee et al. simulated medical problems about the biomechanical effects of dental implant diameter, connection type, and bone density on micro gap formation [29]. In [30], the authors have designed FEM to study the effects of stress and strain distribution in femoral heads for hip resurfacing arthroplasty with different materials. While, on the other hand, the authors simulated FEM to ablate bone tumor by using RFA and succeeded in abating 85% of tumor [31]. In [32], the authors designed FEM to ablate liver tumor by using a cool-tip RF electrode.

Several theoretical studies have studied the effect of the thermal and electrical conductivities of the RF electrode on volume ablation, including both ex-vivo [33, 34] and clinical studies [35, 36]. In [37], the authors compared materials that have high electrical conductivity with those that have low electrical conductivity. In [38], Xu, L., et al simulated RFA model using FEM two cool-tip RF electrodes made of nickel-titanium alloy. Their results showed their success in removing 4 cm^3 of spherical tumor in 10 minutes, and that the best distance between two electrodes when ablation a large tumor is 1 cm. In this paper, we will use that model as a reference model.

The purpose of this paper is to use a computer model to investigate the effect of thermal and electrical conductivity for gamma titanium on ablation volume. In this paper, we designed a model based on the cool-tip RF electrode. The simulation model uses COMSOL Multiphysics software [39] to prove the possibility of reaching this goal. The model is based on a numerical finite element analysis to compute the distribution of heat and electric potential inside the damage and surrounding tissue during an RF ablation. We compared both models (our developed model and the reference model) in the ablation volume values at the same time and with the same power and succeeded in abating large tumors while trying to reduce the damage to healthy cells in less time after using gamma titanium. The research is organized as follows: First, an explanation of the model's methodology, including its equations and parameters; second, the model's results and discussions, highlighting the differences in results between our model and others; and finally, the conclusions.

2. Methods

2.1 FEM Modeling

Each FEM model is included within a cylinder domain that contains both the liver domain and the electrode domain. The radius of the base of the cylinder is 5 cm, the height is 12 cm, and the distance between the two electrodes is 1 cm, adopted to [38]. Each one has the electrode geometry, RF electrode material, and liver tissue to implement. This model has four domains: the liver, electrode, trocar, and tumor domains. Finally, the effect of the following tuning parameters: distance between two electrodes, ablation power, ablation time, and electrode design on the ablation volume is studied.

2.1.1 Liver domain

The liver domain includes everything surrounding the electrode, including blood, blood vessels, and liver tissues. In our study, we assumed that the tumor was spherical as 56% of liver cancer patients had spherical tumors [40]. We assumed that the tumor size was 16 cm^3, which is the largest volume that has been recorded for a liver tumor in Egypt in the last ten years [41].

It stands out for both its high flexibility, which prevents breaking or deformation, both of which pose concerns for patient safety, and its exceptional resistance to rust and corrosion. The inner tube for brine injection that is responsible for cooling is ignored by the suggested model.

2.1.2 Electrode domains

The electrode domain consists of an electrode domain and a trocar domain as shown in figure 1 [38]. The RF electrode consists of:

- An insulated stainless-steel trocar with a diameter of 0.73 mm and a height of 12 cm.
- A nickel-titanium alloy (nitinol) electrode with a height of 3 cm and a diameter of 0.73 mm with a tip in a cone.

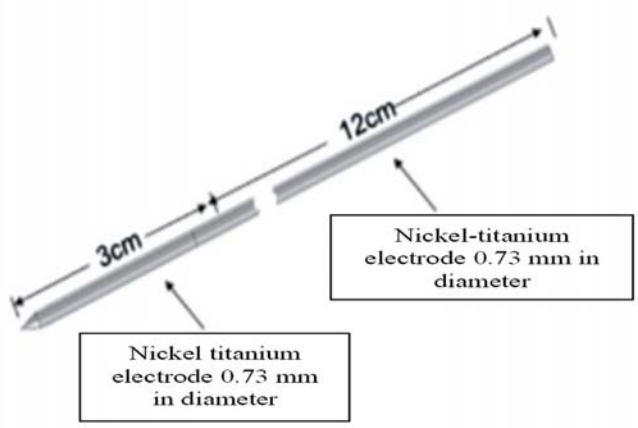

FIGURE 1: A simplified model shows the design of the electrode [38].

2.1.3 Mathematical Equations

2.1.3.1 Bioheat equation

Tissue temperature change due to RF can be mathematically explained by the following Pennes equation [42].

$$\rho c \frac{\partial T}{\partial t} = \nabla \cdot (k \nabla T) - \rho_b c_b \omega_b (T - T_b) + Q_m + JE + Q_b \quad (1)$$

$$JE = \sigma |\nabla V^2| \quad (2)$$

$$Q_b = \omega_b c_b (T_b - T) \quad (3)$$

where ρ is the is the tissue density (kg/m^3), c is tissue specific heat capacity (J/kg/K), k is tissue thermal conductivity (W/m/K), ω_b is blood perfusion rate (1/s), and Q_m is the volumetric heat produced by metabolism (W/ m^3).

JE is joule heating, which represents heat generated by RF, where J is current density, E is electric field intensity, σ is conductivity with a unit of Sm^{-1} and V is voltage impressed on the electrode.

Q_b is volumetric heat produced by radiofrequency heating (Wm^{-3}) calculated using equation (2), T_b is core blood temperature (supposed to be 37°C), because the blood vessels effect was discarded in this study then we can assume T_b and T are equal then $Q_b$was set to zero Wm^{-3}.

2.1.3.2 Electric field

The RF operating frequency is approximately 450-500 kHz, that is usually used for bipolar technique [43]. Depending on this, the main mode of the RF electrode during power delivery is conduction with low capacitance coupling. In this case, the model can be considered as a semi-electrostatic field [44]. The electric field has been calculated using the generalized Laplace equation.

$$\nabla . (\sigma \Delta V) = 0 \quad (4)$$

Where:

σ is (S/m) the electrical conductivity and V is the electric potential (V).

In the model tissues, the losses due to heat contact with the tissues are not significant, so we neglected the losses in our model.

$$E = -\nabla V \quad (5)$$

where ∇ is the operating factor. Then, current density J (A/m^2) is calculated from

$$J = E/\rho e \quad (6)$$

where ρe is the electrical resistivity of the material (Ω m)

Heat of resistance can be generated as a result of the action of an electrical field resulting in the thermal field of the coupling [45]. These two fields have a concerted influence on the division of the heat field and the electric potential field via the liver model [46]. Equations (4)– (6) offer solutions to problems associated with electro-thermal in RFA.

2.1.4 Materials and Boundary Conditions

Depending on the literature, the physical characteristics of the reference model are shown in Table 1.

Table 1. Electrical and thermal properties of the materials [47, 48]

Tissue	Electrical conductivity S/m	Specific heat J/kg.K	Thermal conductivity W/m.K	Density kg/m^3	Blood perfusion s-1
Liver	0.333	3600	0.512	1060	0.0017
Tumor	0.1168	4200	0.552	999	0.0156
Electrode	9.8×10^5	500	36.7	8100	0

Trocar	10^{-16}	1010	0.23	2190	0

The first value voltage and the first value temperature of the whole FEM model were taken as 0 V and 37 ℃, respectively. The liver and tumour have blood perfusion values because they have contact with blood, while the electrode and trocar do not have blood perfusion values because they do not have contact with blood. The surface of the liver was considered insulated and grounded, and the surface of the electrode was voltage loaded V_0 :

$V = 0$ on the surface of the liver (7)

$V = V_0$ on the surface of the electrodes (8)

$n.j = 0$ on all other boundaries (9)

V_0 in our model varied from 22 to 30 volts applied to the RF electrode.

2.1.5 Tuning Parameters of the Model

Understanding the parameters that influence the volume of RF thermal ablation is critical for designing a probe and generator formations that best suit the patient anatomy and clinical goals.

The best way to solve this issue may rely on the application of two RF electrodes. In order to achieve this goal, we have selected three main parameters as follows:

2.1.5.1 Ablation power

Ablation power is related to the amount of energy required to ablate the tumor as follows [49].

$$P = IV = {V^2}/{Z_R} \quad (10)$$

where Z_R is the tissue impedance between RF electrodes.

Usually, the value is 5 joules with direct current charged on the RF electrode [50]. We can increase or decrease the power by changing the value of joules.

2.1.5.2 Ablation time

Time ablation is the time required to perform the ablation process of the tumor [51]. The ablation time ranges from one to ten minutes.

2.1.5.3 Electrode design

The electrode design and its material have an important role in increasing the volume of tumor ablation. In this study, we developed the electrode design by using titanium aluminide alloy (gamma titanium) instead of the nickel-titanium alloy. This titanium alloy is biocompatible and has superior corrosion resistance, high specific strength, rigidity, ~~lower density~~, and higher thermal and electrical conductivities than nitinol, as shown in table 2 [52]. Then, we modified the diameter of the active part from 0.73 mm to 1 mm and the height of the cone from 1 mm to 6 mm to be suitable for large tumors.

Table 2. Properties of the nitinol and gamma titanium materials [53, 54]

Material	Nitinol	Gamma titanium
Electrical conductivity (S/m)	9.8×10^5	9.56×10^6
Specific heat (J/kg.K)	500	620
Thermal conductivity (W/m.K)	36.7	124
Density (kg/m^3)	8100	4700

2.6 Ablated Tissue

Healthy cells are differentiated from ablated cells by calculating the damaged tissue index, α. This index depends on several factors, such as:

- The hyperthermia damage temperature $(T_{d,h})$.
- The cryogenic damage temperature $(T_{d,c})$.
- Instantly after the temperature exceeds the hyperthermia necrosis temperature $(T_{n,h})$.
- Instantly after the temperature falls below the cryogenic necrosis temperature $(T_{n,c})$.

Then the damaged tissue indicator, α, defined either by

$$\alpha = \frac{1}{t_{dh}} \int_0^t \varphi_{d,h} dt \quad (11)$$

$$\alpha = \frac{1}{t_{dc}} \int_0^t \varphi_{d,c} dt \quad (12)$$

where $\varphi_{d,h}$ is the period of time when T > $T_{d,h}$ to the time limit t_{dh} and $\varphi_{d,c}$ the ratio of the period of time when T > $T_{d,c}$ to the time limit t_{dc}.

The value of the damage indices (α) is set to one for healthy cells and zero for damaged cells. When the ablation process starts, damaged cells are removed, and the value is converted from zero to one according to the following equations.

$$\alpha = \begin{cases} 1, & T_{threshold} \geq T_{n,h} \\ 0, & T_{ablation} < T_{n,h}. \end{cases} \quad (13)$$

$$\alpha = \begin{cases} 1, & T_{ablation} \geq T_{n,c} \\ 0, & T_{ablation} < T_{n,c}. \end{cases} \quad (14)$$

After the time of ablation reaches 10 minutes, we computed the ablation volume at various times to evaluate the integrations of areas of damage.

3. Results and Discussion

At the beginning, for both two models, we increased the power value from five joules to 10, 12.5, and 15 joules to increase the ablation volume and decrease the ablation time.

The electric potential field distribution was shown after 10 minutes, as shown in figures 2, 3 and 4. We increased the voltage of the electrical potential value from 3.5 V to 25 V after the development of an RF electrode design, which helps to increase the ablation volume. Then we began to calculate the ablation volume by changing the values for the ablation time and the ablation power. By calculating the ablation volume after the development that we made and comparing it before the development, we found that the ablation volume increased as shown in tables 3, 4, and 5 respectively.

(A)

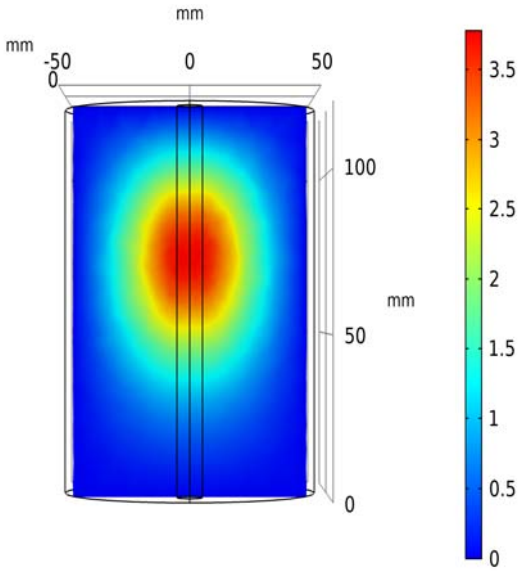

(B)

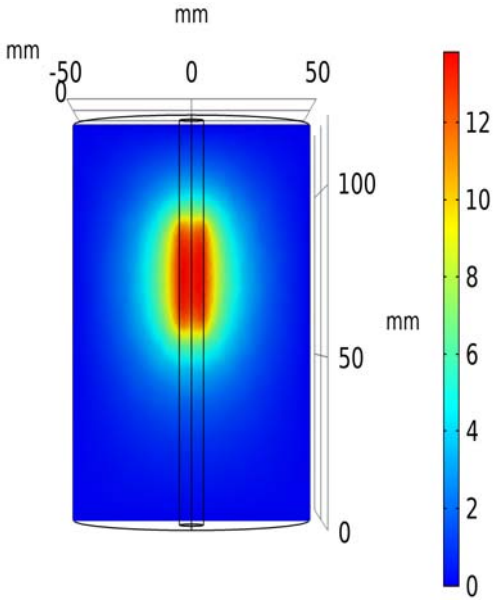

FIGURE 2. Electric potential distribution (A) using nitinol at 10 joules and (B) using gamma titanium at 10 joules.

(A)

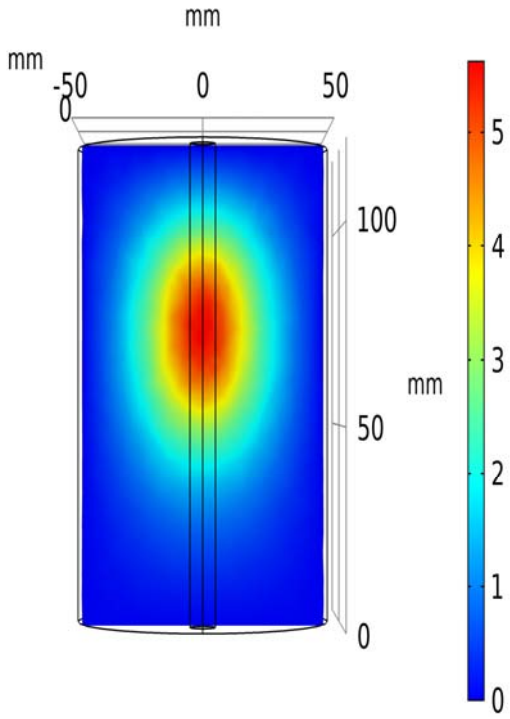

(B)

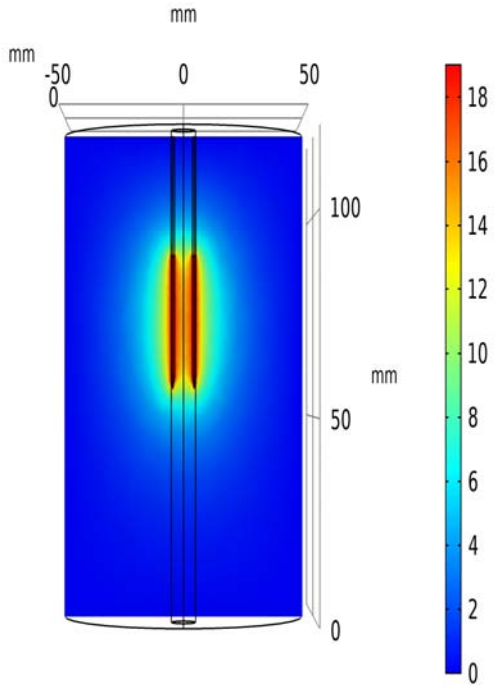

FIGURE 3. Electric potential distribution (A) using nitinol at 12.5 joules and (B) using gamma titanium at 12.5 joules.

(A)

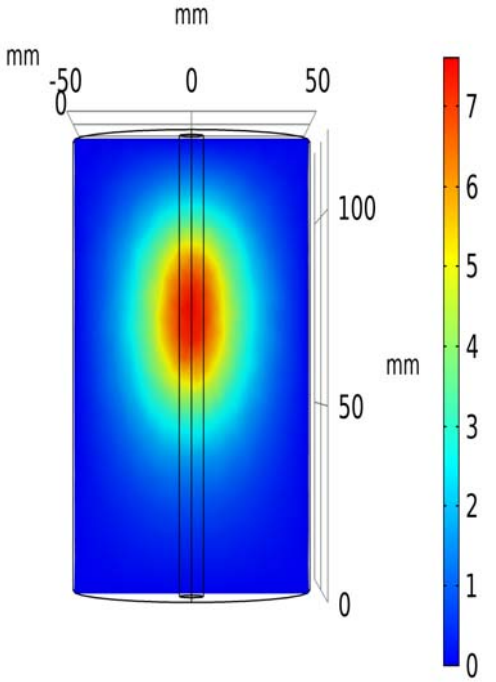

(B)

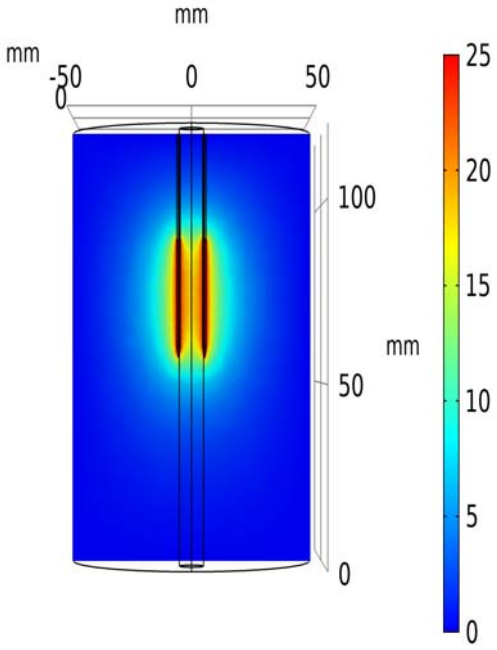

FIGURE 4. Electric potential distribution (A) using nitinol at 15 joules and (B) using gamma titanium at 15 joules.

Table 3. Ablation volume at 10 joules and the rate of increase in the ablation volume.

Time (min)	Volume (cm^3) with a nickel-titanium alloy	Volume (cm^3) with a gamma titanium	Rate of increase (cm^3)
1	0.5	1.4	1
2.5	1.2	2.4	1
5	2.4	3.4	1
7.5	2.9	4.1	1.2
10	3.4	5	1.6

Table 4. Ablation volume at 12.5 joules and the rate of increase in the ablation volume.

Time (min)	Volume (cm^3) with a nickel-titanium alloy	Volume (cm^3) with a gamma titanium	Rate of increase (cm^3)
1	0.5	2.7	2.1
2.5	1.3	4	2.5
5	2.5	5.3	2.9
7.5	3.1	6.5	3.5
10	3.5	7.9	4.3

Table 5. Ablation volume at 15 joules and the rate of increase in the ablation volume.

Time (min)	Volume (cm^3) with a nickel-titanium alloy	Volume (cm^3) with a gamma titanium	Rate of increase (cm^3)
1	0.5	4.9	4.3
2.5	1.4	6.2	4.7
5	2.6	7.5	5
7.5	3.3	8.8	5.7
10	3.6	10	6.3

The simulation results and the percentage of ablation achieved before and after development at 10, 12.5 and 15 joules are shown in figures 5, 6, and 7 respectively.

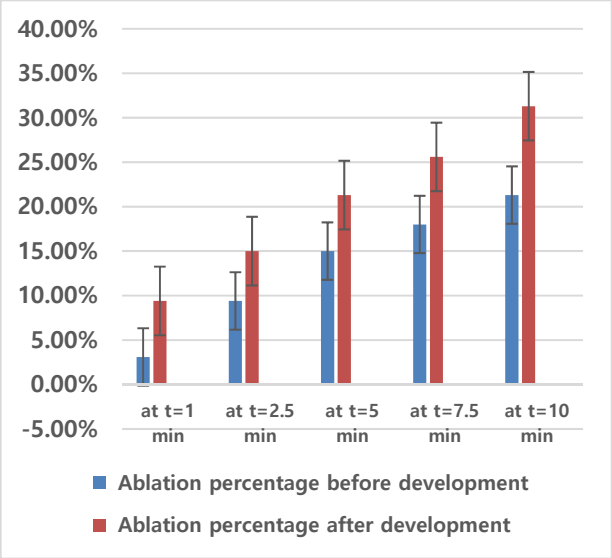

Figure 5. Comparison of ablation percentage before and after adjustments at 10 joules.

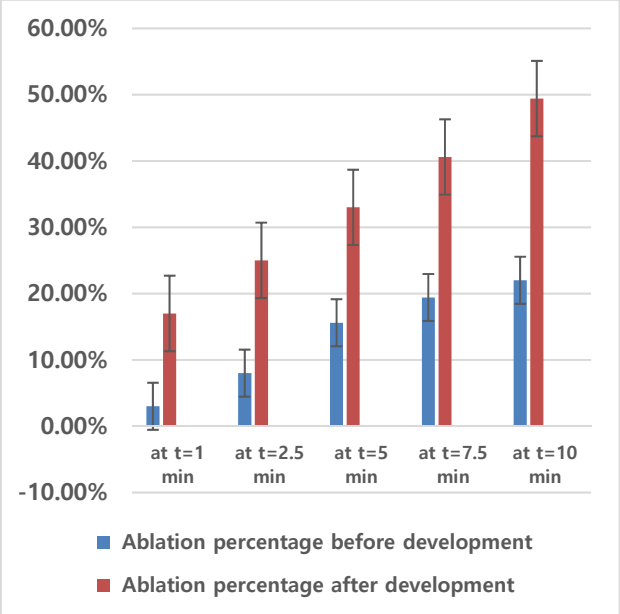

Figure 6. Comparison of ablation percentage before and after development at 12.5 joules.

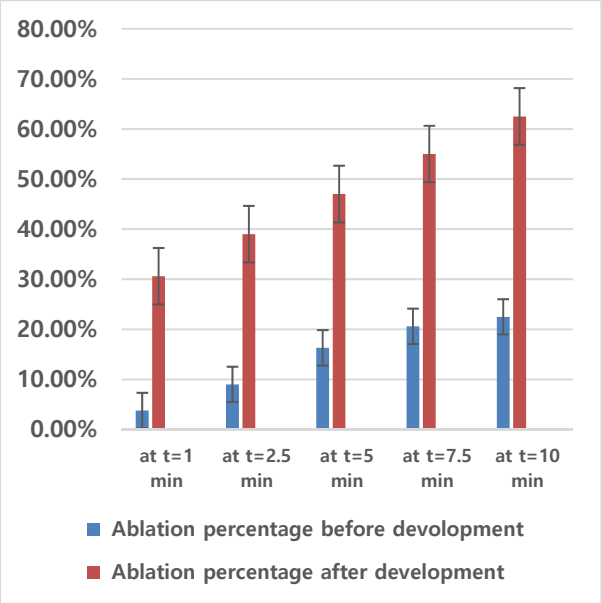

Figure 7. Comparison of ablation percentage before and after development at 15 joules.

It was shown from the results of the new design electrode after development:

- At 10 joules: the maximum ablation volume increased from 3.4 cm^3 to 5 cm^3 and the ablation rate increased from 21.3% to 31.3% after ten minutes of ablation.
- At 12.5 joules: the maximum ablation volume increased from 3.5 cm^3 to 7.9 cm^3 and the ablation rate increased from 22% to 49.4% after ten minutes of ablation.
- At 15 joules: the maximum ablation volume increased from 3.6 cm^3 to 10 cm^3, and the ablation rate increased from 22.5% to 62.5% after ten minutes of ablation.

Using a computer model, we investigated whether gamma titanium electrodes produce greater volume ablation than nitinol electrodes using various RF electrodes at different power levels. We discovered that, with the various power values, the gamma titanium electrodes produced more power in all simulations, leading to greater maximum tissue temperatures and a larger ablation volume with both RF electrodes. We found that the two electrode materials had substantial variances in ablation volume at the same power levels. Consequently, we observed an increase in applied power at the same temperature. While there was a considerable variation in the ablation volumes of the gamma titanium and nitinol

electrode simulations, the gamma titanium electrode produced larger thermal ablation than the nitinol electrode for all power and temperature settings. Gamma titanium and nitinol have different thermal and electrical conductivities, which is probably the source of this. As a result, differences in the characteristics of electrode materials may be advantageous in clinical settings; our modelling findings point to potentially significant advantages.

The impact of gamma titanium electrodes on ablation volume is clearly seen in figure 3, where gamma titanium electrodes were used. Using it shows a big effect on ablation volume but a significant effect on blood temperature, which rises close to 50 °C in the region nearby the RF electrode. The two simulations comparing gamma titanium and nitinol show a clear increase in ablation volume for gamma titanium. A large ablation volume is produced by increased thermal and electrical conductivity. The outcomes of these two simulations can be discussed in light of the application of gamma-titanium electrical conductivity to liver tissue. A graphical result of the simulations is the large extension of ablation volume in the electrode's direction. This is most likely caused by the electrode tip emitting a significantly higher electric current than the rest of the electrode surface. When deciding where to place the electrode, it could be important to take this uneven current distribution into account.

4. Conclusion

The results show that using gamma titanium instead of nickel-titanium achieved an increase in the ablation volume because it has higher electrical and thermal conductivity than nickel-titanium alloy. Also, the results show the effect of tuning parameters (ablation power, ablation time and design of the electrode) on increasing the ablation volume and decreasing the ablation time. The results show that the electrode design is the most important tuning parameter because with the change of design from the reference model to our developed model, the effect and success of the rest of the tunning parameters appeared. That helps to reduce the patient's pain and increase the accuracy. Future work can study the effect of a RF multi-hooks electrodes on large tumors by using the same tuning parameters and compare it with a RF cool-tip electrode.

References

[1] Ostroumov, D., et al., *Transcriptome Profiling Identifies TIGIT as a Marker of T-Cell Exhaustion in Liver Cancer.* Hepatology, 2021. **73**(4): p. 1399-1418.

[2] Tong, J., et al., *Machine Learning Can Predict Total Death After Radiofrequency Ablation in Liver Cancer Patients.* Clinical Medicine Insights: Oncology, 2021. **15**: p. 11795549211000017.

[3] Wah, T.M., et al., *Radiofrequency ablation (RFA) of renal cell carcinoma (RCC): experience in 200 tumours.* BJU international, 2014. **113**(3): p. 416.

[4] Sheng, W., et al., *Clinical application of a three-dimensional reconstruction technique for complex liver cancer resection.* Surgical Endoscopy, 2021: p. 1-8.

[5] Minami, Y. and M. Kudo, *Radiofrequency ablation of hepatocellular carcinoma: a literature review.* International journal of hepatology, 2011. **2011**.

[6] Ghomashchi, S., et al., *Impact of radiofrequency ablation (RFA) on bone quality in a murine model of bone metastases.* Plos one, 2021. **16**(9): p. e0256076.

[7] Pregel, P., et al., *Radiofrequency thermoablation on ex vivo animal tissues: changes on isolated swine thyroids.* Frontiers in Endocrinology, 2021. **12**: p. 697.

[8] Mauri, G., et al., *Benign thyroid nodules treatment using percutaneous laser ablation (PLA) and radiofrequency ablation (RFA).* International journal of hyperthermia, 2017. **33**(3): p. 295-299.

[9] Nour-Eldin, N.-E.A., et al., *Ablation therapy of non-colorectal cancer lung metastases: retrospective analysis of tumour response post-laser-induced interstitial thermotherapy (LITT), radiofrequency ablation (RFA) and microwave ablation (MWA).* International Journal of Hyperthermia, 2017. **33**(7): p. 820-829.

[10] Lucchina, N., et al., *Current role of microwave ablation in the treatment of small hepatocellular carcinomas.* Annals of Gastroenterology: Quarterly Publication of the Hellenic Society of Gastroenterology, 2016. **29**(4): p. 460.

[11] Hocquelet, A., et al., *Comparison of no-touch multi-bipolar vs. monopolar radiofrequency ablation for small HCC.* Journal of hepatology, 2017. **66**(1): p. 67-74.

[12] Al-Alem, I., et al., *Heat sink phenomenon of bipolar and monopolar radiofrequency ablation observed using polypropylene tubes for vessel simulation.* Surgical Innovation, 2014. **21**(3): p. 269-276.

[13] Chang, W., et al., *No-touch radiofrequency ablation: a comparison of switching bipolar and switching monopolar ablation in ex vivo bovine liver.* Korean journal of radiology, 2017. **18**(2): p. 279-288.

[14] Huang, Y.-Z., et al., *Radiofrequency ablation versus cryosurgery ablation for hepatocellular carcinoma: a meta-analysis.* Hepato-gastroenterology, 2013. **60**(125): p. 1131-1135.

[15] Li, L., et al., *Clinical outcomes of radiofrequency ablation and surgical resection for small hepatocellular carcinoma: A meta-analysis.* Journal of gastroenterology and hepatology, 2012. **27**(1): p. 51-58.

[16] Song, T.J., et al., *Initial experience of EUS-guided radiofrequency ablation of unresectable pancreatic cancer.* Gastrointestinal endoscopy, 2016. **83**(2): p. 440-443.

[17] Goode, S., et al., *Laser and radiofrequency ablation study (LARA study): a randomised study comparing*

radiofrequency ablation and endovenous laser ablation (810 nm). European Journal of Vascular and Endovascular Surgery, 2010. **40**(2): p. 246-253.

[18] Albers, F., et al., *Functional mri readouts from bold and diffusion measurements differentially respond to optogenetic activation and tissue heating.* Frontiers in neuroscience, 2019. **13**: p. 1104.

[19] Webb, H., M.G. Lubner, and J.L. Hinshaw. *Thermal ablation*. in *Seminars in roentgenology*. 2011. Elsevier.

[20] Titi, M., et al., *Development of subsquamous high-grade dysplasia and adenocarcinoma after successful radiofrequency ablation of Barrett's esophagus.* Gastroenterology, 2012. **143**(3): p. 564-566. e1.

[21]Vallejo, R., et al., *An ex vivo comparison of cooled-radiofrequency and bipolar-radiofrequency lesion size and the effect of injected fluids.* Regional Anesthesia & Pain Medicine, 2014. **39**(4): p. 312-321.

[22] Monteiro, M., et al. *Evaluation of Cytotoxicity of Nickel-Titanium Electrode for Hepatic Ablation Equipment with Carcinosarcoma Walker 256 Tumor Model*. in *XXVI Brazilian Congress on Biomedical Engineering*. 2019. Springer.

[23] Močnik, P. and T. Kosec, *A Critical Appraisal of the Use and Properties of Nickel–Titanium Dental Alloys.* Materials, 2021. **14**(24): p. 7859.

[24] Wen, S., et al., *Research status and prospect of additive manufactured nickel-titanium shape memory alloys.* Materials, 2021. **14**(16): p. 4496.

[25] Eliaz, N., *Corrosion of metallic biomaterials: A review.* Materials, 2019. **12**(3): p. 407.

[26] Stintzing, S., et al., *Percutaneous radiofrequency ablation (RFA) or robotic radiosurgery (RRS) for salvage treatment of colorectal liver metastases.* Acta oncologica, 2013. **52**(5): p. 971-977.

[27] Rozenblum, N., et al., *Oncogenesis: an "off-target" effect of radiofrequency ablation.* Radiology, 2015. **276**(2): p. 426-432.

[28] Reddy, J.N., *Introduction to the finite element method*. 2019: McGraw-Hill Education.

[29] Lee, H., M. Jo, and G. Noh, *Biomechanical effects of dental implant diameter, connection type, and bone density on microgap formation and fatigue failure: A finite element analysis.* Computer Methods and Programs in Biomedicine, 2021. **200**: p. 105863.

[30] Vogel, D., et al., *Stress and strain distribution in femoral heads for hip resurfacing arthroplasty with different materials: A finite element analysis.* Journal of the Mechanical Behavior of Biomedical Materials, 2021. **113**: p. 104115.

[31] Ramírez-Guzmán, T., et al. *Design of a Cooling System for Micro-coaxial Antennas in the Treatment of Bone Tumours without Affecting the Ablation Zone: FEM Models*. in *2021 Global Medical Engineering Physics Exchanges/Pan American Health Care Exchanges (GMEPE/PAHCE)*. 2021. IEEE.

[32] Radmilović-Radjenović, M., et al., *Finite element analysis of the microwave ablation method for enhanced lung cancer treatment.* Cancers, 2021. **13**(14): p. 3500.

[33] Mulier, S., et al., *Radiofrequency ablation with four electrodes as a building block for matrix radiofrequency ablation: Ex vivo liver experiments and finite element method modelling. Influence of electric and activation mode on coagulation size and geometry.* Surgical Oncology, 2020. **33**: p. 145-157.

[34] Bourier, F., et al., *Impedance, power, and current in radiofrequency ablation: insights from technical, ex vivo, and clinical studies.* Journal of Cardiovascular Electrophysiology, 2020. **31**(11): p. 2836-2845.

[35] Lee, J., et al., *Feasibility of adjustable electrodes for radiofrequency ablation of benign thyroid nodules.* Korean Journal of Radiology, 2020. **21**(3): p. 377-383.

[36] Nakagawa, H., et al., *Comparison of in vivo tissue temperature profile and lesion geometry for radiofrequency ablation with high power–short duration and moderate power–moderate duration: effects of thermal latency and contact force on lesion formation.* Circulation: Arrhythmia and Electrophysiology, 2021. **14**(7): p. e009899.

[37] Baldelli, A., et al., *Sprayable, superhydrophobic, electrically, and thermally conductive coating.* Advanced Materials Interfaces, 2021. **8**(2): p. 1902110.

[38] Xu, L., et al., *Simulation of multi-probe radiofrequency ablation guided by optical surgery navigation system under different active modes.* Computer Assisted Surgery, 2016. **21**(1): p. 107-116.

[39] Multiphysics, C. *COMSOL Multiphysics® 5.4*. COMSOL Multiphysics 2021; Available from: https://www.comsol.com/.

[40] Mahnič-Kalamiza, S. and D. Miklavčič, *Scratching the electrode surface: Insights into a high-voltage pulsed-field application from in vitro & in silico studies in indifferent fluid.* Electrochimica Acta, 2020. **363**: p. 137187.

[41] Attia, M.S., et al., *A new method for early diagnosis of liver cancer using a biosensor embedded in an alginate polymer thin film.* Journal of Materials Chemistry C, 2022. **10**(16): p. 6464-6472.

[42] Ghazanfarian, J., R. Saghatchi, and D. Patil, *Implementation of smoothed-particle hydrodynamics for non-linear Pennes' bioheat transfer equation.* Applied Mathematics and Computation, 2015. **259**: p. 21-31.

[43] Nadakuduti, J., L. Lu, and P. Guckian. *Operating frequency selection for loosely coupled wireless power transfer systems with respect to RF emissions and RF exposure requirements*. in *2013 IEEE Wireless Power Transfer (WPT)*. 2013. IEEE.

[44] Sun, J.-Y., et al., *The effects of electron surface interactions in geometrically symmetric capacitive RF plasmas in the presence of different electrode surface materials.* Physics of Plasmas, 2019. **26**(6): p. 063505.

[45] Mercer, R., et al., *Genetic determinants of heat resistance in Escherichia coli.* Frontiers in microbiology, 2015. **6**: p. 932.

[46] Nagarajan, V., A.K. Mohanty, and M. Misra, *Perspective on polylactic acid (PLA) based sustainable materials for durable applications: Focus on toughness and heat resistance.* ACS Sustainable Chemistry & Engineering, 2016. **4**(6): p. 2899-2916.

[47] Ooi, E.H., et al., *The effects of electrical and thermal boundary condition on the simulation of radiofrequency ablation of liver cancer for tumours located near to the liver boundary.* Computers in biology and medicine, 2019. **106**: p. 12-23.

[48] Yap, S., et al., *Comparisons between impedance-based and time-based switching bipolar radiofrequency ablation for*

the treatment of liver cancer. Computers in biology and medicine, 2021. **134**: p. 104488.
[49] Egashira, Y., et al., *Percutaneous high-energy microwave ablation for the treatment of pulmonary tumors: a retrospective single-center experience.* Journal of Vascular and Interventional Radiology, 2016. **27**(4): p. 474-479.
[50] Wang, X.-K., et al., *The effect of a negative direct-current voltage on striated structures and electrical parameters in a capacitively coupled rf discharge in CF4.* Plasma Sources Science and Technology, 2021. **30**(5): p. 055019.
[51] Liu, L., et al., *Detection of distant metastasis at the time of ablation in children with differentiated thyroid cancer: the value of pre-ablation stimulated thyroglobulin.* Journal of Pediatric Endocrinology and Metabolism, 2018. **31**(7): p. 751-756.
[52] Baltatu, M.S., et al., *Biocompatible titanium alloys used in medical applications.* Rev. Chim, 2019. **70**(4): p. 1302-1306.
[53] Mantcheva, R., et al., *Biocompatibility of aluminium alloys and anodic Al2O3.* BULGARIAN CHEMICAL COMMUNICATIONS, 2017. **49**(2): p. 371-376.
[54] Patil, V., S. Balivada, and S. Appagana, *Biomedical Applications of Titanium and Aluminium based High Entropy Alloys.* International Journal of Health Technology and Innovation, 2022. **1**(01): p. 40-48.